Acta Pharmaceutica Sinica B 2023;13(2):852–862

Chinese Pharmaceutical Association
Institute of Materia Medica, Chinese Academy of Medical Sciences

Acta Pharmaceutica Sinica B

www.elsevier.com/locate/apsb
www.sciencedirect.com

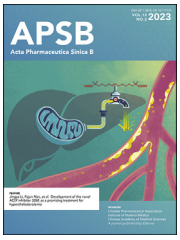

ORIGINAL ARTICLE

# Precise assembly of inside-out cell membrane camouflaged nanoparticles *via* bioorthogonal reactions for improving drug leads capturing

**Xiaolin Zhang[a,b], Xueyan Zhen[a,b], Yixuan Yang[a,b], Quan Feng[a,b], Wanqing Yuan[a,b], Xiaoyu Xie[a,b,*]**

[a]*School of Pharmacy, Health Science Center, Xi'an Jiaotong University, Xi'an 710061, China*
[b]*Shaanxi Engineering Research Center of Cardiovascular Drugs Screening & Analysis, Xi'an 710061, China*

Received 20 February 2022; received in revised form 4 April 2022; accepted 17 May 2022

**KEY WORDS**

Cell membrane camouflaged nanoparticles;
Inside-out cell membrane coating;
Bioorthogonal reactions;
Drug leads discovery;
Traditional Chinese medicine;
Magnetic nanoparticles;
Precise assembly;
Alkynyl functionalization

**Abstract** Cell membrane camouflaged nanoparticles have been widely used in the field of drug leads discovery attribute to their unique biointerface targeting function. However, random orientation of cell membrane coating does not guarantee effective and appropriate binding of drugs to specific sites, especially when applied to intracellular regions of transmembrane proteins. Bioorthogonal reactions have been rapidly developed as a specific and reliable method for cell membrane functionalization without disturbing living biosystem. Herein, inside-out cell membrane camouflaged magnetic nanoparticles (IOCMMNPs) were accurately constructed *via* bioorthogonal reactions to screen small molecule inhibitors targeting intracellular tyrosine kinase domain of vascular endothelial growth factor recptor-2. Azide functionalized cell membrane acted as a platform for specific covalently coupling with alkynyl functionalized magnetic $Fe_3O_4$ nanoparticles to prepare IOCMMNPs. The inside-out orientation of cell membrane was successfully verified by immunogold staining and sialic acid quantification assay. Ultimately, two compounds, senkyunolide A and ligustilidel, were successfully captured, and their potential antiproliferative activities were further testified by pharmacological experiments. It is anticipated that the proposed inside-out cell membrane coating strategy endows tremendous versatility for engineering cell membrane camouflaged nanoparticles and promotes the development of drug leads discovery platforms.

*Corresponding author. School of Pharmacy, Health Science Center, Xi'an Jiaotong University, Xi'an 710061, China.
E-mail address: xiexiaoyu@xjtu.edu.cn (Xiaoyu Xie).

Peer review under responsibility of Chinese Pharmaceutical Association and Institute of Materia Medica, Chinese Academy of Medical Sciences

https://doi.org/10.1016/j.apsb.2022.05.034

## 1. Introduction

Cell membrane with complete biological structure and dynamic lateral fluidity has been directly used as a kind of natural biomaterial to encapsulate nanoparticles[1−3]. Cell membrane camouflaged nanoparticles display multiple desirable characteristics such as long blood circulation[4,5], superior ligand targeting capability[6,7] and enhanced particle stability[8,9]. In particular, a great number of proteins and carbohydrates on the cell membrane surface mediate a wide range of biological interactions. Among them, receptors can selectively combine with drugs *in vivo,* accounting for over two-thirds of drug targets[10−12]. On account of this, cell membrane camouflaged nanoparticles have emerged as a promising platform for capturing potential bioactive ingredients in complex matrices[13−15]. However, considering the asymmetry properties of cell membrane and the well-defined orientation of transmembrane proteins[16,17], maintaining the controllability of cell membrane orientation is of great significance in promoting the discovery of bioactive compounds.

Especially, receptor tyrosine kinases (RTKs) are single-pass transmembrane glycoproteins composed of an N-terminal extracellular domain, a single transmembrane helix region and an intracellular kinase domain, which play a critical role in the development process and deterioration of multiple cancers[18−20]. Small molecule tyrosine kinase inhibitors can act on highly conserved intracellular kinase domain of RTKs to inhibit tyrosine phosphorylation[21]. Therefore, the development of inside-out cell membrane camouflaged nanomaterials to provide intracellular kinase domain is urgently needed. Thus far, lipid insertion method has been utilized to construct drug screening materials with an inside-out cell membrane coating[22]. Nevertheless, there are tremendous challenges for the usage of lipopolymers functionalized cell membrane, mainly resulting from unstable connection relied on physical interactions[23]. Particularly, the lipid−polymer conjugates rapidly disappear from cell membrane due to hydrophobic interaction between free proteins and lipid anchor[24,25]. Consequently, exploring engineering method with better coupling stability and biocompatibility is a key challenge for the accurate construction of cell membrane camouflaged nanoparticles with inside-out orientation and may eventually facilitate the discovery of small molecule tyrosine kinase inhibitors.

Recently, bioorthogonal reactions have been developed as new powerful tools for selective modification of active biomolecules *in vitro* or *in vivo* owing to its high specificity and non-interfering with other components[26,27]. The functional derivatives such as unnatural monosaccharide can effectively incorporate various chemical groups including azide, alkyne and cyclopropane into glycan on the cell surface through cellular metabolic pathway[28]. Importantly, these exogenous "artificial chemical receptors" can be subsequently modified with specific cross-linked groups through bioorthogonal reactions. At present, bioorthogonal reactions have been widely applied in bioimaging[29,30], tumor-targeting[31,32] and glycobiology[33,34] due to their advantages such as no impact on cell viability and functions, mild physiological conditions and high yield[35]. Base on this, we envisioned that cellular intrinsic metabolic pathway could provide an excellent functional groups for efficient fabrication of inside-out cell membrane camouflaged nanoparticles through bioorthogonal reactions, which could be applied to screen small molecule tyrosine kinase inhibitors and overcome the limitation of instability of lipid insertion methods.

In this contribution, we proposed a well-designed inside-out cell membrane camouflaged platform through bioorthogonal reactions for screening drug leads from nature products. Briefly, the azide analogues were introduced into the surface of high-expression vascular endothelial growth factor recptor-2 (VEGFR-2)/HEK293 cells by metabolic glycoengineering. Then, inside-out cell membrane camouflaged magnetic nanoparticles (IOCMMNPs) could be achieved on the basis of the specific bioorthogonal reactions between the unnatural azide groups located on the outside of the cell membrane and the corresponding alkynyl functionalized magnetic nanoparticles. We systematically evaluated and characterized the orientation of cell membrane coating of IOCMMNPs including immunogold staining and sialic acid quantification assay. Additionally, a series of characterizations, adsorption performances and screening procedure of IOCMMNPs have been thoroughly evaluated. Compared to random direction cell membrane camouflaged magnetic nanoparticles (RCMMNPs), IOCMMNPs showed better adsorption capacity because more adsorption sites were exposed. Eventually, the developed IOCMMNPs were successfully applied for the targeted screening of bioactive compounds from *Ligusticum chuanxiong* Hort with high sensitivity. The inside-out cell membrane camouflaging technology further expands the wide application of bioorthogonal reactions and provides a potential platform for site-specific drug targeted screening.

## 2. Materials and methods

### 2.1. Materials and regents

Sodium citrate, anhydrous sodium acetate, ethylene glycol, tetraethoxy silane (TEOS), 3-aminopropyltriethoxysilane (APTES), Iron (III) chloride hexahydrate ($FeCl_3 \cdot 6H_2O$), propiolic acid, 4-methylpyridine (DMAP) and dicyclohexylcarbodiimide (DCC) were provided by Macklin Technology Co., Ltd. (Shanghai, China). *N*-Azidoacetylmannosamine-tetraacylated ($Ac_4$ManNAz) was supplied by Xi'an ruixi Biological Technology Co., Ltd. (Xi'an, China). DBCO-Cy5 was offered by Sigma−Aldrich LLC. (St. Louis, MO, USA). 1,1′-Dioctadecyl-3,3,3′,3′-tetramethylindocarbocyanine perchlorate (DiI) was offered from Beyotime Biotechnology Co., Ltd. (Shanghai, China). Fluorescein isothiocyanate isomer (FITC) was purchased from MedChemExpress (Princeton, NJ, USA). CD47 antibodies and C-term CD47 antibodies were purchased from GeneTex, Inc. (Irvine, CA, USA). Colloidal gold labeled secondary antibodies was offtered by Sigma−Aldrich LLC.. Sorafenib, dexamethasone, nifedipine, gliclazide and tamsulosin were provided by Sinopharm Chemical Reagent Co., Ltd. (Xi'an, China). Senkyunolide A and ligustilide were supplied by Yuan Ye Biological Technology Co., Ltd.

(Shanghai, China). *L. chuanxiong* Hort was offered by Yi Kang Medicine (Xi'an, China). Acetonitrile, isopropyl alcohol and DMSO (HPLC grade solvents) were provided from Thermo Fisher Scientific (Waltham, MA, USA).

### 2.2. Preparation of IOCMMNPs

$Fe_3O_4$, $Fe_3O_4$@$SiO_2$ and $Fe_3O_4$@$SiO_2$@$NH_2$ magnetic nanoparticles were synthesized according to the protocol previously described[36], details of which were shown in supporting information. The preparation process of $Fe_3O_4$@$SiO_2$@$NH_2$@C≡CH (denoted as bare MNPs) was as follows[37]. 1 g $Fe_3O_4$@$SiO_2$@$NH_2$ was dispersed in 33 mL dichloromethane, followed by the addition of 745 μL propiolic acid, 0.13 g DMAP and 2.2 g DCC. The reaction mixtures were stirred for 24 h under $N_2$ atmosphere at 120 °C. Finally, the obtained products were magnetically collected and then washed three times with ethanol and ultrapure water in turn.

The high-expression VEGFR-2 cell lines were constructed with engineering cell HEK293 according to the method proposed in a Chinese patent (authorized No.: CN 101701209 B). The high-expression VEGFR-2/HEK293 cells were cultured in DMEM medium−high glucose supplemented with 10% fetal bovine serum (FBS) and 1% streptomycin-penicillin antibiotic at 37 °C and 5% $CO_2$. The cells were incubated with azido sugar ($Ac_4$ManNAz, 50 μmol/L) for 48 h at 37 °C. Then, the cells were disengaged with 0.25% trypsin/EDTA solution, and separated at 1000×*g* for 10 min, and gently washed three times with 1 × phosphate-buffered saline (PBS, pH 7.4) buffer solution. Subsequently, the collected cells were soaked in Tris−HCl (50 mmol/L, pH 7.4) with ultrasound for 30 min. Cell pellets were centrifuged at 1000×*g* for 10 min at 4 °C, then supernatant was collected and centrifuged at 12,000×*g* for 20 min. The azide-functionalized VEGFR-2/HEK293 cell membrane ($N_3$-cell membrane) was resuspended in PBS buffer and frozen at −80 °C.

The prepared bare MNPs were sufficiently dispersed in $N_3$-cell membrane suspension. Then 1 μL freshly prepared catalytic solution (400 mmol/L $CuSO_4$, 800 mmol/L sodium ascorbate and 200 mmol/L TBTA) was added to the mixture systems, and which were stirred at 1400 rpm for 30 min at room temperature to prepare IOCMMNPs. As a control, RCMMNPs were prepared by sufficiently fusing bare MNPs with VEGFR-2/HEK 293 cell membrane suspension (without the labeling of azide functional groups) under vacuum ultrasound at 4 °C for 15 min. Moreover, HEK293 cell membrane was selected as a negative control because HEK293 cells do not express exogenous VEGFR-2 (the result of its expression levels was shown in Supporting Information Fig. S1), which was coated on the surface of bare MNPs magnetic nanoparticles (HCMMNPs). The details of the preparation material characterization were described in supporting information.

### 2.3. Validation of metabolically labeled VEGFR-2/HEK293 cells

To determine azide groups were grafted on the surface of high-expression VEGFR-2/HEK293 cells, 3 × $10^4$ cells were seeded in 35 mm glass-bottom dishes with incubated with $Ac_4$ManNAz (50 μmol/L). After incubation for 48 h, the metabolite-treated VEGFR-2/HEK293 cells were washed twice with 1 × PBS buffer (pH 7.4) and subsequently treatment of 20 μmol/L DBCO-Cy5 at 37 °C for 2 h. The labeled high-expression VEGFR-2/HEK293 cells (Cy5-VEGFR-2/HEK293 cells) were softly washed twice with 1 × PBS buffer (pH 7.4), and then fixed with 4% paraformaldehyde (PFA) for 15 min. After fixation, the cells were stained with DAPI solution (Yeasen, Shanghai, China) to label nuclei for 3 min and visualized using super-resolution confocal laser scanning microscope (CLSM, Leica, TCS SP8 STED 3X, Solms, Germany).

### 2.4. Determination of cell membrane coverage

$N_3$-cell membrane was stained with DiI, and bare MNPs were stained with FITC. Then IOCMMNPs were prepared according to the above method, and the images were observed and analyzed under fluorescence microscope. Moreover, membrane proteins of IOCMMNPs were evaluated by sodium dodecyl sulfate-polyacrylamide gel electrophoresis (SDS-PAGE). In short, VEGFR-2/HEK293 cells, $N_3$-cell membrane and IOCMMNPs were lysed on ice with RIPA lysis buffer (Epizyme Biomedical Technology Co., Ltd, Shanghai, China) and the total protein concentrations were determined by BCA protein concentration assay kit (Beyotime Biotechnology Co., Ltd.,). The equivalent protein contents were loaded in 8% SDS-PAGE gel and then separated. Finally, the gel was stained with Coomassie blue G-250 dye for 1 h and destained with distilled water overnight for imaging analysis.

### 2.5. Determination of cell membrane orientation

The immunogold staining and sialic acid quantification assay were used to evaluate cell membrane orientation. For immunogold staining, IOCMMNPs, RCMMNPs and bare MNPs solution were dropped on the carbon-copper grid, respectively. The grid was washed with PBS (pH7.4), blocked in a 5% bovine serum albumin (BSA) buffer, and then incubated with anti-CD47 antibodies for 30 min that specifically integrated into the intracellular or extracellular region of CD47. Subsequently, the sample was washed with 0.5% BSA solution and then stained with colloidal gold labeled secondary antibodies solution for another 30 min. The droplet sample was rinsed with water and visualized using transmission electron microscopy (TEM, JEOL, JEM2100F, Tokyo, Japan).

Cell membrane orientation was also studied by sialic acid quantification assay. IOCMMNPs were incubated with sialidase in water at room temperature for 2 h to dissociate the sialic acid from the cell membrane surface, and subsequently centrifuged at 200,000×*g* for 45 min using a Himac CP-NX ultracentrifuge (Koki Holdings Co., Ltd., Tokyo, Japan). The supernatant was then collected and using a sialic acid quantification kit (Sigma−Aidrich LLC.) to examine sialic acid content. The same amounts of cell membrane ghost (CM ghost), RCMMNPs and bare MNPs were treated with the same protocol, respectively.

### 2.6. Adsorption experiments

To assess the adsorption property of IOCMMNPs, static, dynamic and selectivity adsorption experiments were performed. Sorafenib was choosed as positive drug, due to it is a small molecule VEGFR-2 tyrosine kinase inhibitor.

The adsorption isotherm experiments were performed by adding 5 mg IOCMMNPs, RCMMNPs, bare MNPs and HCMMNPs into 1 mL sorafenib solution with many different concentrations (40−3000 mg/L), respectively. The residual concentration of sorafenib in supernatant after adsorption was analyzed by HPLC. The adsorption ability ($Q$, mg/g) equation as shown in Eq. (1):

$$Q=\frac{(C_o-C_e)\times V}{m} \quad (1)$$

where $C_o$ (mg/L) and $C_e$ (mg/L) represents the initial concentration and the final concentration of sorafenib. $V$ (mL) is the volume of analyte solution. $m$ (mg) refers to the amount of IOCMMNPs, RCMMNPs, bare MNPs and HCMMNPs.

In adsorption kinetics tests, IOCMMNPs, RCMMNPs, bare MNPs and HCMMNPs were dispersed in 1 mL sorafenib solution (200 mg/L), respectively. The supernatant was collected at certain time intervals (10 s−25 min) and detected by HPLC. The adsorption amounts were also calculated by Eq. (1).

To evaluate the specific recognition property of IOCMMNPs, sorafenib, acting on VEFGR-2, was selected as a positive drug. Some drugs that do not act on VEGFR-2 were selected as negative controls, such as gliclazide (a hypoglycemic agent that acts on sulfonylurea receptors), nifedipine (a dihydropyridine calcium channel blocker), dexamethasone (a glucocorticoid receptor agonist) and tamsulosin (a selective $\alpha_1$ adrenoceptor antagonist). In short, 5 mg IOCMMNPs, RCMMNPs, bare MNPs and HCMMNPs were mixed with 1 mL each standard ligand (100 mg/L), respectively. Afterwards, the amounts of unbound drugs in supernatant were determined by HPLC, which was also calculated by Eq. (1).

### 2.7. *Real application of IOCMMNPs*

Potential active ingredients screened from traditional Chinese medicine (TCM) have been used to treat various diseases[38,39]. Thus, the prepared IOCMMNPs were putted into TCM extracts solutions to investigate its practical application performance. 8 g *L. chuanxiong* Hort was ground into fine powder and then reflux extracted with 50 mL 70% ethanol for 2 h. Then the obtained total extracts were dried by evaporation and redissolved with 1 mL methanol. IOCMMNPs (5 mg) were incubated with the extract for 15 min to adsorb potential bioactive compounds bound to cell membrane receptors. Subsequently, IOCMMNPs, collected by a magnetic field, were washed with water-acetonitriler solution (7:3, *v*/*v*). Lastly, the potential bioactive compounds were eluted by DMSO and identified by gas chromatography-mass spectrometer (GC−MS, Shimadzu Corporation, Kyoto, Japan).

### 2.8. *Cell viability assay*

Cell Counting Kit-8 (CCK-8) assay was applied to assess the inhibitory effect of the obtained bioactive compounds on VEGFR-2/HEK293 cells. In short, cells were dispensed in a 96-well plates containing $1 \times 10^4$ cells per well. Then they were treated with different concentrations of sorafenib, senkyunolide A and ligustilide for 48 h, respectively. Subsequently, 10 μL of CCK-8 stock reagents (YESEN Biotechnology Co., Ltd., Shanghai, China) was added to per well and then incubated for 30 min. Finally, the optical density was measured at 450 nm by a microplate reader.

### 2.9. *Western blot analysis*

Total proteins were obtained from VEGFR-2/HEK293 cells using RIPA lysis buffer, and the protein concentration of samples was measured by BCA protein assay kit. The proteins were then loaded and separated by SDS-PAGE with 10% polyacrylamide gel and then transferred onto polyvinylidene fluoride (PVDF) membrane. After being blocked in 5% skim milk for 2 h at room temperature, the PVDF membrane was kept overnight at 4 °C with primary antibodies against VEGFR-2 (#2479, 1:1000, *v*/*v*, CST), phosphorylated-VEGFR-2 (p-VEGFR-2) (#2478, 1:1000, *v*/*v*, CST), protein kinase B (AKT) (#4685, 1:1000, *v*/*v*, CST), phosphorylated-AKT (p-AKT) (#4060, 1:1000, *v*/*v*, CST), extracellular regulated protein kinases (ERK) (#4695, 1:1000, *v*/*v*,

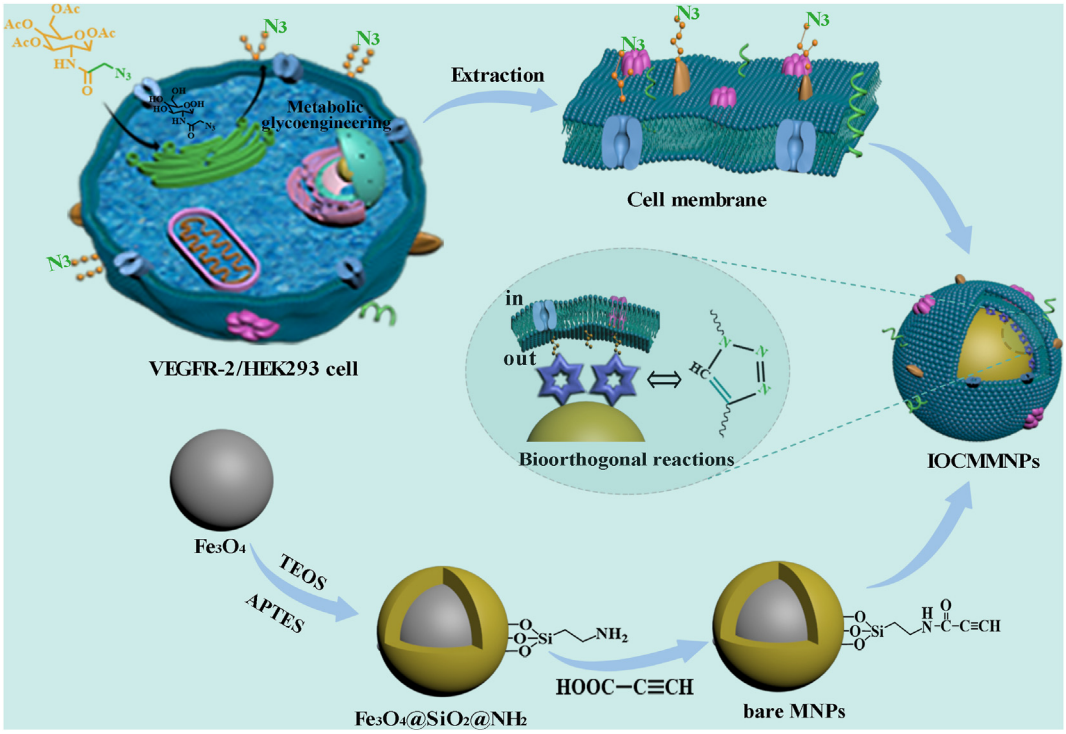


**Figure 1** Schematic representation of the preparation process of IOCMMNPs.

CST), phosphorylated-ERK (p-ERK) (#4370, 1:1000, *v/v*, CST) and glyceraldehyde phosphate dehydrogenase (GAPDH) (#5174, 1:1000, *v/v*, CST). The PVDF membrane was then incubated with horseradish peroxidase (HRP)-conjugated secondary antibodies (#7074, 1:3000, *v/v*, CST) for 1 h at 37 °C, and the immunoreactive bands were visualized by enhanced chemiluminescence (ECL) reagent. All signals were quantitatively analyzed by Image J software (National Institutes of Health, MD, USA).

## 3. Results and discussion

### 3.1. Metabolism of azide groups on the surface of VEGFR-2/HEK293 cells

As a typical RTKs, the precise assembly of VEGFR-2 guarantees the effectivity and applicability of drug binding sites. Bioorthogonal reactions have attracted considerable attention in the field of live cell labeling and tracking and was therefore applied for inside-out cell membrane cloaking in this work. The schematic representation of the preparation process was shown in Fig. 1. At first, VEGFR-2/HEK293 cells were treated with azido sugar ($Ac_4ManNAz$) to produce abundant exogenous azide groups on the cell surface through intracellular metabolic glycoengineering. After that, the synthesized bare MNPs were coated with the resulting azide groups-cell membrane by bioorthogonal reactions.

It was crucial that azide groups were metabolized on the cells surface. Near-infrared fluorescent dye (DBCO-Cy5), which could be specifically conjugated to azide groups by bioorthogonal reactions, was selected to prove the incorporation of azide groups on the surface of cells. As depicted in Fig. 2A, the $Ac_4ManNAz$ + DBCO-Cy5 group emitted strong red fluorescence signal on the cells surface, while no obvious red fluorescence was detected in the DBCO-Cy5 group without incubation with $Ac_4ManNAz$. The CLSM results demonstrated that the azide groups were successfully inserted onto the surface of cells.

### 3.2. Characterization of IOCMMNPs

Fourier transform infrared spectroscopy (FTIR) spectra of $Fe_3O_4$ (a), $Fe_3O_4@SiO_2$ (b), $Fe_3O_4@SiO_2@NH_2$ (c) and bare MNPs (d) were displayed in Fig. 2B. The characteristic band of Fe−O stretching vibration of $Fe_3O_4$ was located at 572 $cm^{-1}$ (curve a). The characteristic peaks of $Fe_3O_4@SiO_2$ (curve b) were observed at 800, 950, and 1085 $cm^{-1}$, which were belonged to the Si−O, Si−O−H and Si−O−Si stretching vibration, respectively. Although the bands of $Fe_3O_4@SiO_2@NH_2$ (curve c) were same as those of $Fe_3O_4@SiO_2$, the characterization of $Fe_3O_4@SiO_2@NH_2$ was demonstrated by other methods. In bare MNPs (curve d), the characteristic peak at 3322 $cm^{-1}$ was corresponded to C−H stretching vibration of alkyne. Moreover, X-ray photoelectron spectroscopy (XPS) was executed to characterize the surface groups and elements of prepared composites. As depicted in Fig. 2C, the peak of N 1s in $Fe_3O_4@SiO_2@NH_2$ (curve a) was obviously observed, confirming the successful modification of

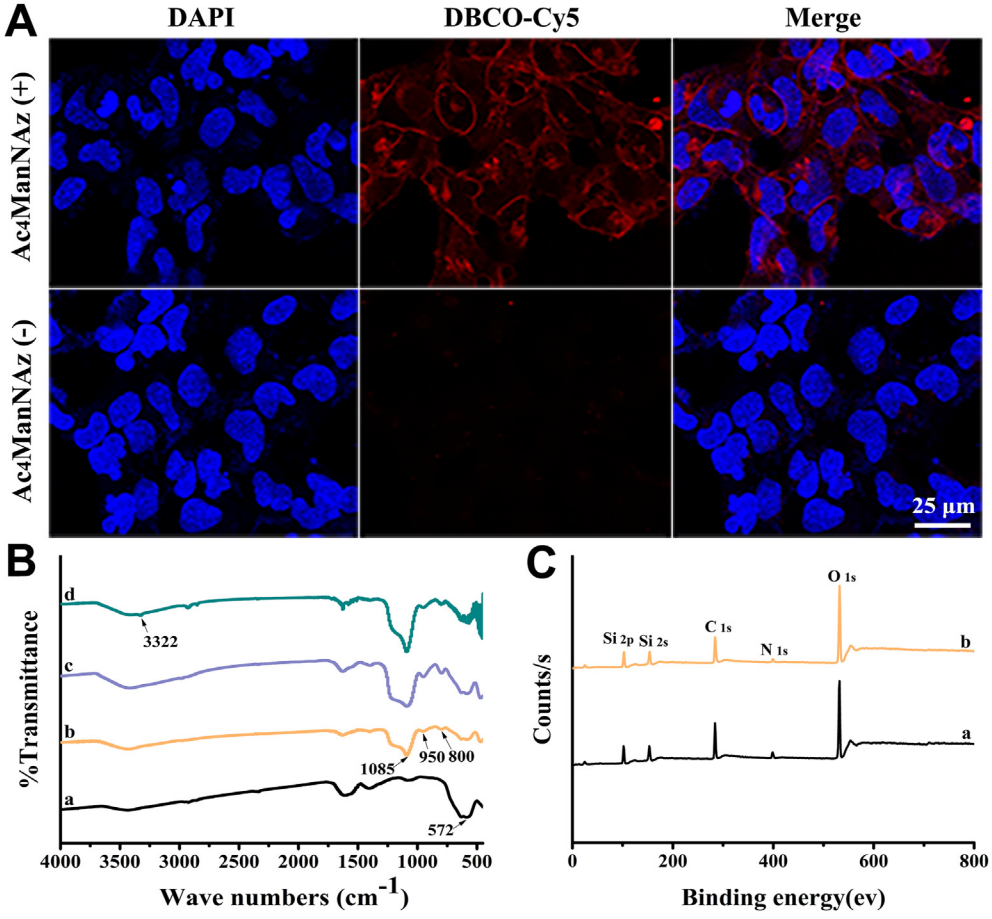


**Figure 2** (A) CLSM images of VEGFR-2/HEK293 cells treated and untreated with $Ac_4ManNAz$. Scale bar = 25 μm. (B) FTIR spectra of $Fe_3O_4$ (a), $Fe_3O_4@SiO_2$ (b), $Fe_3O_4@SiO_2@NH_2$ (c) and bare MNPs (d). (C) XPS patterns of $Fe_3O_4@SiO_2@NH_2$ (a) and bare MNPs (b).

$NH_2$ on $Fe_3O_4$@$SiO_2$. The peaks of bare MNPs (curve b) were similar to those of $Fe_3O_4$@$SiO_2$@$NH_2$, suggesting that there was no change in the elemental composition during the preparation process.

The measurement results of dynamic light scattering exhibited that the particle size increased after being coated with $SiO_2$ (c), as well as bare MNPs (d), RCMMNPs (e) and IOCMMNPs (f) had similar size distributions (Supporting Information Fig. S2). Moreover, after cell membrane coating, the surface charges of the obtained materials (e and f) was similar to that of cell membrane vesicles (a), and the Zeta potential of IOCMMNPs was lower than that of RCMMNPs (Supporting Information Fig. S3), which could be attributed to the lipids and proteins distributions on the both sides of the cell membrane are apparently different.

The crystal structures of $Fe_3O_4$ (a), $Fe_3O_4$@$SiO_2$ (b), $Fe_3O_4$@$SiO_2$@$NH_2$ (c), bare MNPs (d) and IOCMMNPs (e) were observed by X-ray diffraction (XRD) in Supporting Information Fig. S4. Six characteristic diffraction peaks corresponding to (220), (311), (400), (422), (511) and (440) were observed in all samples at $2\theta = 30.3°$, $35.6°$, $43.3°$, $53.7°$, $57.4°$ and $62.7°$, respectively, which indicated that the magnetite crystalline phase remained unchanged during the preparation of the composites. Magnetic property measurement system (MPMS) was used to measure the magnetic properties of the prepared composites at room temperature (Supporting Information Fig. S5). The saturation magnetization (Ms) values of 41.85 and 32.80 emu/g for bare MNPs and IOCMMNPs, respectively, which were lower than Ms values of $Fe_3O_4$ (58.59 emu/g). Although Ms values were somewhat reduced due to chemical functional groups modification and cell membrane coating, IOCMMNPs still had enough magnetic responsiveness to ensure rapid separation through the additional magnetic fields.

### 3.3. *Envelope of cell membrane*

The successful coating of the $N_3$-cell membrane on the carrier material is of great significance for the practical application of IOCMMNPs. To verify the covering of $N_3$-cell membrane, bare MNPs was labeled with FITC and then incubated with DiI-labeled $N_3$-cell membrane. As shown in Fig. 3A, the green fluorescence originated from the labeled nanoparticles (a) overlapped perfectly with the red fluorescence from the labeled $N_3$-cell membrane (b), indicating that $N_3$-cell membrane successfully coated on the surface of carrier materials. Moreover, the retention of cell membrane receptors is essential for targeting ligands. As shown in Fig. 3B, cell lysate (a), cell membrane (b) and IOCMMNPs (c) had similar protein compositions analyzed by SDS-PAGE. The results suggested that cell membrane proteins almost remained during the preparation of IOCMMNPs.

The inside-out orientation of cell membrane is critical for subsequent practical application of IOCMMNPs. CD47 is a transmembrane protein widely expressed on the surface of human cells, consisting of an N-terminal extracellular region, five hydrophobic transmembrane helix structures and a very short C-terminal intracellular sequence[40], which can be acted as a properly indicator to identify the cell membrane orientation of IOCMMNPs. As shown in Fig. 3C, TEM visualization showed that several electron-dense gold particles were attached to intracellular anti-CD 47 labeled IOCMMNPs (a), while no gold particles were accumulated on extracellular anti-CD 47 labeled IOCMMNPs (b). The results

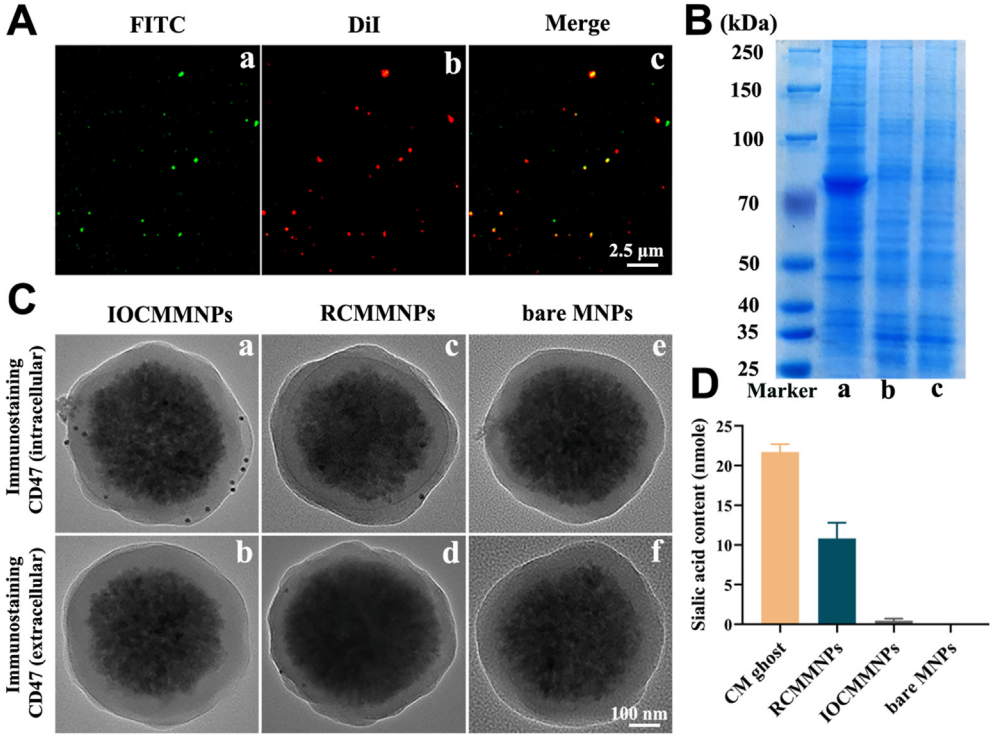


**Figure 3** Characterization of IOCMMNPs coverage and orientation. (A) Fluorescence colocalization images of IOCMMNPs. Scale bar = 2.5 μm. (B) Proteins analysis of cell lysate (a), cell membrane (b) and IOCMMNPs (c) by SDS-PAGE. (C) TEM images of IOCMMNPs, RCMMNPs and bare MNPs with extracellular or intracellular domains of CD47 indicated by immunogold labeling. Scale bar = 100 nm. (D) Determination of sialic acid content in CM ghost, RCMMNPs, IOCMMNPs and bare MNPs. Data were presented as mean ± SD ($n = 3$).

demonstrated that the cell membrane orientation of IOCMMNPs was inside-out. For RCMMNPs randomly coated with cell membrane, a small amount of aggregation immune gold particles could be observed on the surface (c and d). For bare MNPs, no aggregation immune gold particles were observed (e and f). Moreover, sialic acid, present exclusively on the extracellular surface of asymmetric cell membrane[41], was further quantitatively analyzed. As shown in Fig. 3D, the sialic acid content in CM ghost group was much higher than that in RCMMMNPs group, whereas there was no sialic acid in IOCMMNPs and bare MNPs groups. The results demonstrated that IOCMMNPs were prepared by an inside-out cell membrane coating approach.

### 3.4. *Adsorption capacity*

The isotherm adsorption experiments were performed to evaluate the adsorption capacity of adsorbents. The adsorption amounts of IOCMMNPs, RCMMNPs, bare MNPs and HCMMNPs at different concentrations of sorafenib were presented in Fig. 4A. Obviously, with the increase of sorafenib concentration, the adsorption capacity of the four sorbents also increased, and reached saturation at 1500 mg/L. In addition, the maximum binding amounts of IOCMMNPs, RCMMNPs, bare MNPs and HCMMNPs were 370.4, 210.7, 19.2 and 12.9 mg/g, respectively. It was implied that the adsorption ability of IOCMMNPs for sorafenib was stronger than those of RCMMNPs, bare MNPs and HCMMNPs, which could be attributed to IOCMMNPs possessed cell membrane with inside-out, resulting in more specific receptors exposure. To deeply study the binding properties of adsorbents, Freundlich, Langmuir, Scatchard and Dubinin−Radushkevich isotherm models were used to process the binding data. As shown in Supporting Information Table S1 and Fig. S6, the binding process of IOCMMNPs could be more fitted to Freundlich isotherm model [correlation coefficient ($r$) = 0.9912] than other models, which suggested that sorafenib could be

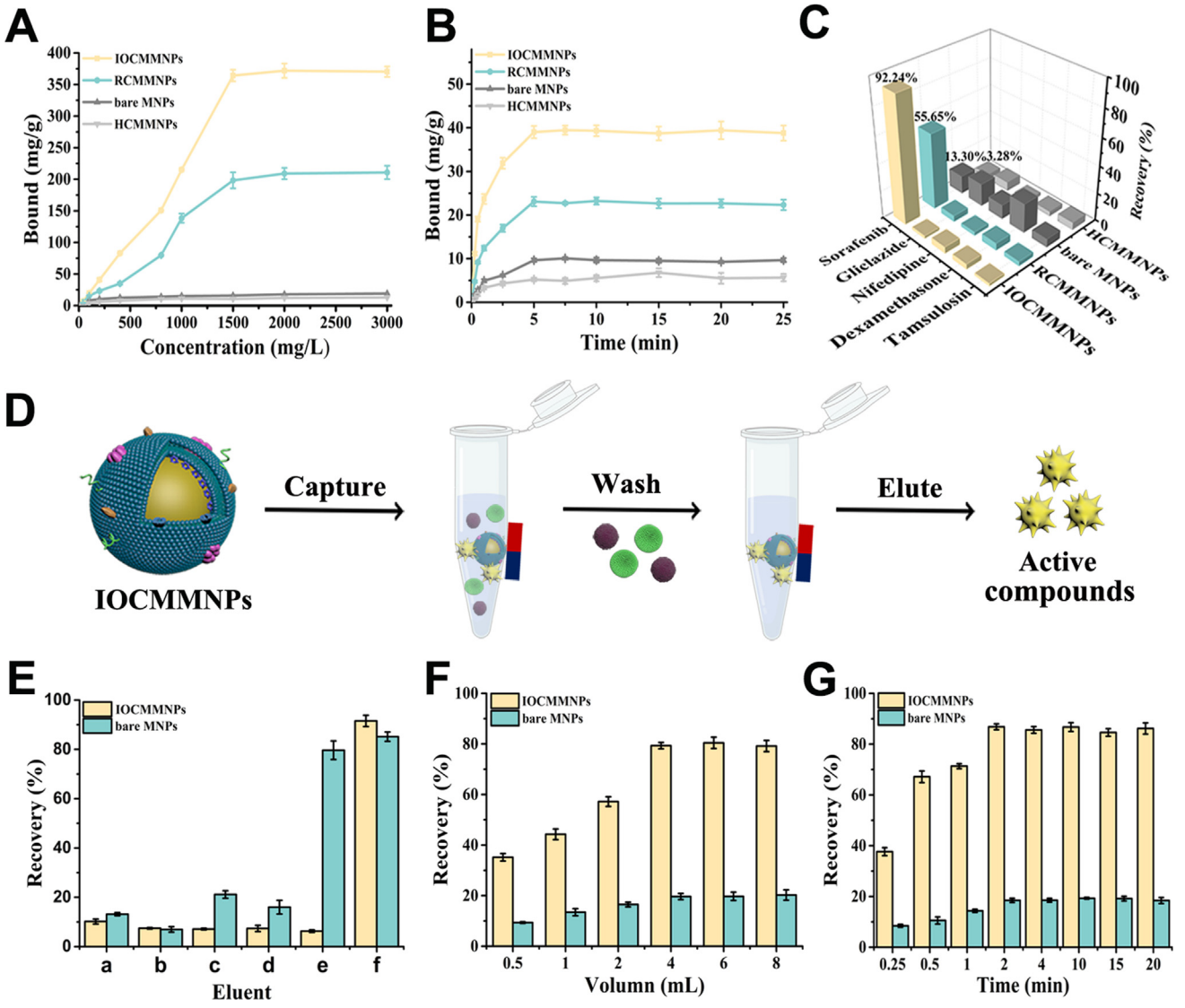


**Figure 4** (A) Isotherm adsorption experiments of IOCMMNPs, RCMMNPs, bare MNPs and HCMMNPs. (B) Adsorption kinetics of IOCMMNPs, RCMMNPs, bare MNPs and HCMMNPs. (C) Adsorption selectivity of IOCMMNPs, RCMMNPs, bare MNPs and HCMMNPs. (D) Schematic diagram of optimized capture conditions. (E) Selection of washing and elution solutions: water (a), PBS (b), water−acetonitrile (c, 9:1, *v*/*v*), water−isopropanol (d, 9:1, *v*/*v*), water−acetonitrile (e, 7:3, *v*/*v*) and DMSO (f). (F) Investigation of elution volume. (G) Investigation of elution time.

reversibly adsorbed on the heterogeneous solid surface of IOCMMNPs[42].

### 3.5. *Adsorption kinetics*

The adsorption kinetics of adsorbents for sorafenib were illustrated in Fig. 4B, which presented an initial significantly increase in the first 5 min and then reached saturation. As time increased, the adsorption sites were gradually occupied until adsorption saturation was reached. Meanwhile, IOCMMNPs kept a higher binding amount than those of RCMMNPs, bare MNPs and HCMMNPs, which was due to the presence of more adsorption sites on the surface of IOCMMNPs for sorafenib. To further examine the adsorption process of the prepared materials, pseudo-first-order (PFO) and pseudo-second-order (PSO) models were applied to analyze the kinetic data of adsorbents. As listed in Supporting Information Table S2, for IOCMMNPs, the correlation coefficient of PSO model ($r = 0.9927$) was higher than that of PFO model ($r = 0.9232$), suggesting that chemical adsorption possibly dominated the binding process between receptor of IOCMMNPs and sorafenib.

### 3.6. *Adsorption selectivity*

The selective recognition ability of IOCMMNPs was essential for practical applications. To this end, the adsorption selectivity of IOCMMNPs, RCMMNPs, bare MNPs and HCMMNPs for five drugs was investigated. These include the positive drug (sorafenib) and four negative drugs (gliclazide, nifedipine, dexamethasone and tamsulosin) that act on other receptors. The results were shown in Fig. 4C. It was clearly observed that both IOCMMNPs and RCMMNPs showed good adsorption capacity for sorafenib, among which IOCMMNPs had the highest adsorption capacity. However, IOCMMNPs and RCMMNPs showed low binding amounts for the four negative drugs, and there was no remarkable difference in adsorption amounts. In addition, there was no significant difference in the adsorption ability of bare MNPs and HCMMNPs for the five drugs. The above results indicated that VEGFR-2/HEK293 cell membrane played a crucial role in the selective recognition of sorafenib, and the inside-out orientation of cell membrane coating could increase the adsorption sites for sorafenib.

### 3.7. *Optimization of screening procedure*

Appropriate screening procedures and conditions are important for effective target acquisition. After the extracts loading, the inactive compounds, adsorbed by nonspecific forces, needed to be washed (Fig. 4D). As shown in Fig. 4E, there were significant differences about recoveries of sorafenib under different elution solvents. Good desorption effect for bare MNPs was obtained using water−acetonitrile (e, 7:3, *v*/*v*), but only a weak desorption effect for IOCMMNPs. Moreover, most sorafenib was eluted from both IOCMMNPs and bare MNPs using DMSO (f). Therefore, water−acetonitrile (7:3, *v*/*v*) was selected as washing solutions and DMSO was chosen as elution solutions.

Furthermore, the eluent volume and elution time were also optimized. As shown in Fig. 4F, with the volume increased from 0.5 to 4 mL, the recovery of IOCMMNPs for sorafenib increased. When the volume was greater than 4 mL, the recovery remained constant. In addition, the elution time was investigated from 0.25 to 20 min (Fig. 4G). The recovery of IOCMMNPs for sorafenib increased from 0.25 to 2 min and then remained stable. As a

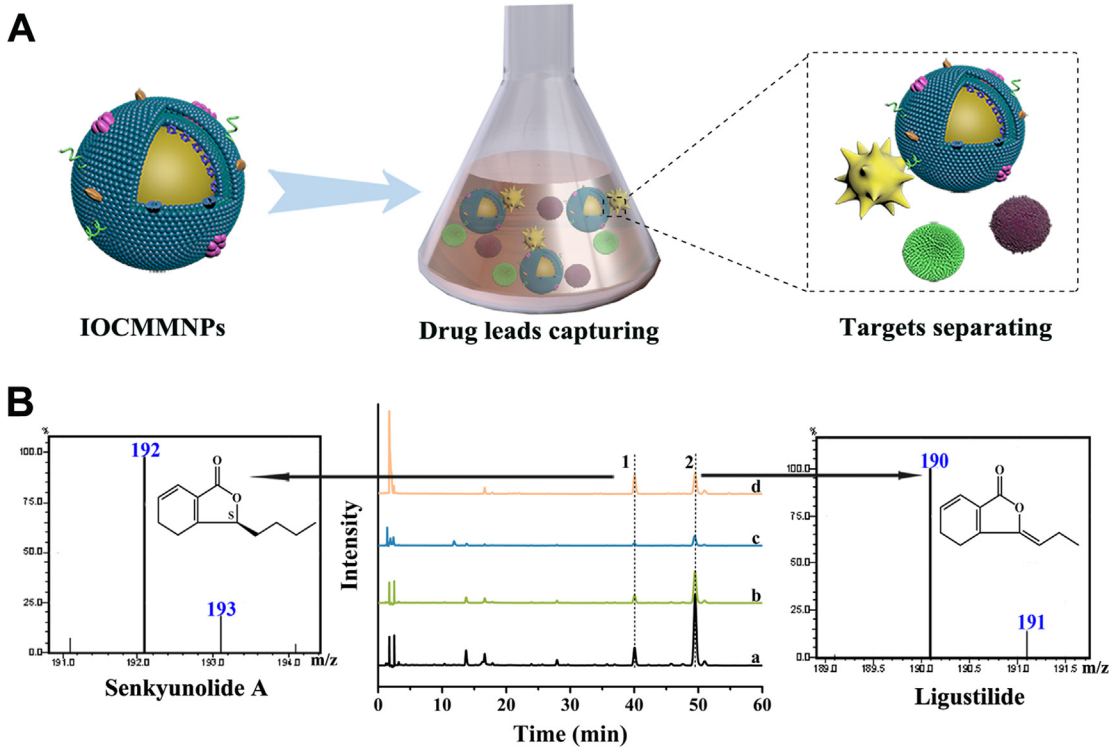


**Figure 5** (A) Schematic illustration of IOCMMNPs for capturing drug leads. (B) Chromatograms of the practical application using IOCMMNPs: extract solution (a), solution after loading (b), solution after washing (c) and solution after eluting (d); GC−MS results of peaks 1 and 2.

result, the optimal elution volume was 4 mL, and the optimal elution time was 2 min.

### 3.8. *Method validation and application in complex herbal matrices*

To evaluate the analytical parameters of the developed method, sorafenib was used as a reference to evaluate the following parameters, including linearity, limit of detection (LOD) and method precision. The linear range was determined to be 0.05−50 μg/mL with $r = 0.9999$, and the LOD ($S/N = 3$) was calculated as 0.8 ng/mL. The results suggested that the present method possessed good sensitivity and met the needs of detection. Furthermore, six batches of IOCMMNPs were used to determine the method precision. The results displayed that the relative standard deviation (RSD) of recoveries was 1.71%, which could be considered that the method had high precision and reproducibility, and could be used in practical application.

To verify that the proposed platform could be applied for rapid screening of active ingredients in complex matrices, IOCMMNPs were used to capture drug leads from the extract of *L. chuanxiong* Hort (Fig. 5A). The results were depicted in Fig. 5B. It could be clearly observed that only a few components could be remained on IOCMMNPs after loading of the extraction solution (b). After rinsing with wash and elution solvent, two main peaks were detected in the eluent solution (d), its might be the potential bioactive components captured by IOCMMNPs. These two compounds were recoginized as senkyunolide A and ligustilide by GC−MS. Hence, the prepared IOCMMNPs could be applied to screen bioactive compounds acted on VEGFR-2 tyrosine kinase from complex TCMs.

### 3.9. *Pharmacological effect*

To assess the inhibitory property of above two components, VEGFR-2/HEK293 cells were treated with senkyunolide A and ligustilide with different concentrations (5−35 μg/mL), and cell viability was evaluated using CCK-8 assy. As depicted in Fig. 6A, the results showed that senkyunolide A and ligustilide dose-dependently inhibited cell growth. Moreover, the half-maximal inhibitory concentration ($IC_{50}$) of senkyunolide A and ligustilide were 19.81 and 21.22 μg/mL, respectively. Thus, it revealed that two bioactive compounds could effectively inhibit proliferation of VEGFR-2/HEK293 cells.

Dimerization and phosphorylation of VEGFR-2 can activate multiple downstream signaling pathways, including AKT and ERK, etc[43]. The effects of senkyunolide A and ligustilide on the protein expression and phosphorylation levels of VEGFR-2, AKT and ERK

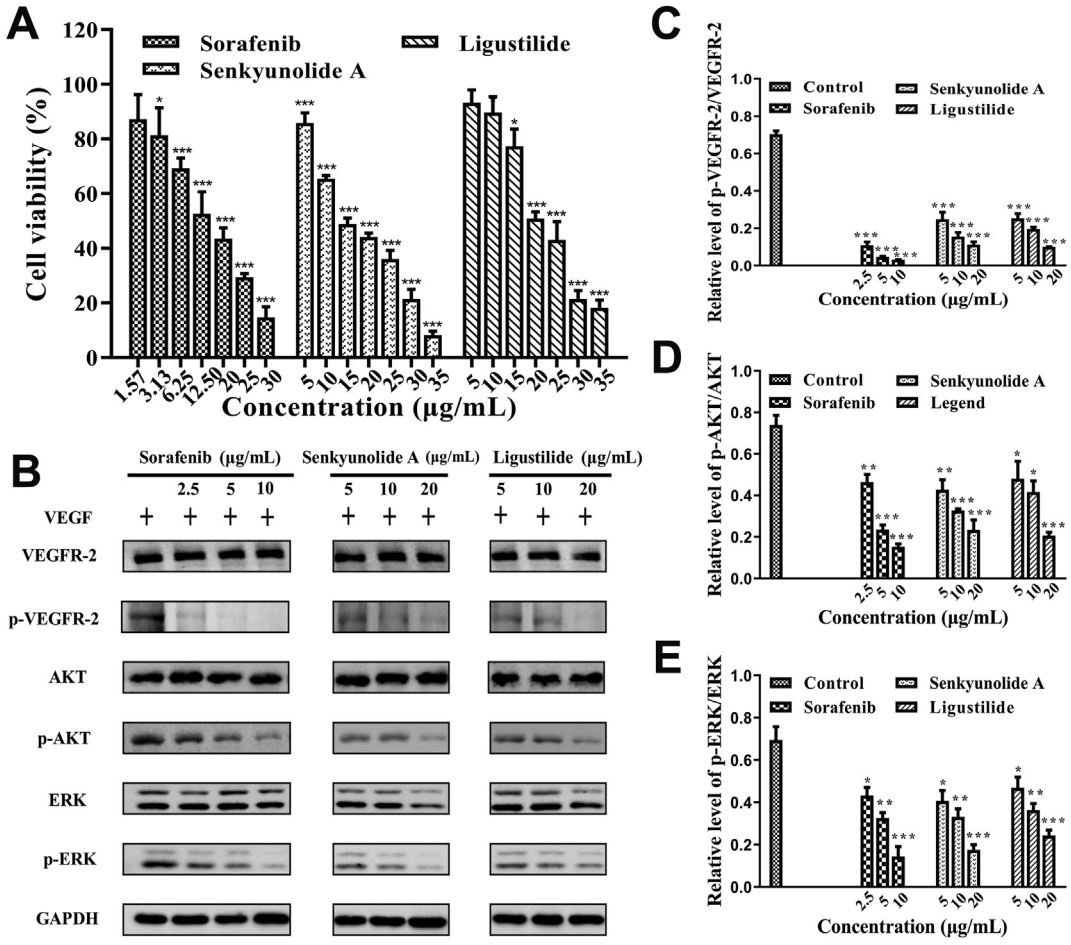


**Figure 6** (A) Cell viability of VEGFR-2/HEK293 cells treated with sorafenib, senkyunolide A and ligustilidel. (B) The expression of related proteins in VEGFR-2/HEK293 cells treated with sorafenib, senkyunolide A and ligustilidel. (C) The relative level of p-VEGFR-2/VEGFR-2. (D) The relative level of p-AKT/AKT. (E) The relative level of p-ERK/ERK. Data are presented as mean ± SD ($n = 3$). *$P < 0.05$, **$P < 0.01$ and ***$P < 0.001$ *vs*. control group.

in the VEGFR-2/HEK293 cells were examined *via* western blotting experiments. As displayed in Fig. 6B, senkyunolide A and ligustilide dose-dependently reduced the expression of p-VEGFR-2, while the expression of VEGFR-2 was almost unaffected. The results showed that these two compounds inhibited VEGF-induced phosphorylation of AKT and ERK (p-AKT and p-ERK), but the protein expression levels of AKT and ERK showed no obvious dose-dependent changes. Moreover, the quantification results in Fig. 6C−6E demonstrated that the phosphorylation levels of VEGFR-2, AKT and ERK were significantly reduced after treatment with senkyunolide A and ligustilide compared with the control group. Our results indicated that senkyunolide A and liguslide could inhibit VEGFR-2/HEK293 cells proliferation by down-regulating VEGFR-2 phosphorylation pathway.

### *3.10. Interaction simulations of screened compounds with VEGFR-2*

The molecular docking study was performed to explore the interaction mechanism of screened compounds and VEGFR-2. Sorafenib, an ATP-competitive inhibitor, was first docked with VEGFR-2 (PDB ID: 3WZE), and then senkyunolide A and liguslide were docked with VEGFR-2 under the same method conditions. As shown in Supporting Information Figs. S7A, S8A and S9A, senkyunolide A and ligustilide showed similar activity binding pockets to sorafenib. Moreover, detailed analysis of the interactions between the potential active ingredients and VEGFR-2 were shown in the striped results (Fig. S7B, Fig. S8B and Fig. S9B). Senkyunolide A formed a hydrogen bond with CYS919 in VEGFR-2, which was consistent with a hydrogen bond of sorafenib. These docking results demonstrated that senkyunolide A and ligustilide were identified as selective VEGFR-2 tyrosine kinase inhibitors.

## 4. Conclusions

In this work, we designed a novel inside-out cell membrane coating strategy with better biocompatibility and stability based on bioorthogonal reactions for drug leads discovery. The outside surface of cell membrane was specifically labeled with azide functional groups through metabolic engineering, which was further covalently reacted with the alkynyl groups of magnetic nanoparticles. It has been verified that the inside-out coating method not only improved the adsorption capacity of the target, but also helped to determine the action sites of drug. Moreover, two potential active ingredients, senkyunolide A and ligustilidel, were successfully screened from *L. chuanxiong* Hort. Preliminary pharmacological results suggested that both compounds could inhibit VEGFR-2 phosphorylation and further block downstream signaling pathways, thereby inhibiting tumor cell proliferation. In summary, the inside-out cell membrane cloaking strategy based on bioorthogonal reactions provides a powerful tool for precise immobilization of cell membrane, and also opens up a new horizon for effective screening of drug leads from natural products.

## Acknowledgments

We gratefully acknowledge the National Natural Science Foundation of China (No. 82073807). And we thank for Dr Jiamei Liu and Dr Ying Hao at the Instrument Analysis Center of Xi'an Jiaotong University for their assistance with XPS and CLSM analysis.

## Author contributions

Xiaolin Zhang carried out the experiments, analyzed the data and wrote the manuscript. Xueyan Zhen, Yixuan Yang, Quan Feng and Wanqing Yuan participated part of the experiments. Xiaoyu Xie designed the study and revised the manuscript. All of the authors have read and approved the final manuscript.

## Conflicts of interest

The authors declare no conflicts of interest.

## Appendix A. Supplementary data

Supplementary data to this article can be found online at https://doi.org/10.1016/j.apsb.2022.05.034.

## References

1. Zhao QQ, Sun XY, Wu B, Shang YH, Huang XY, Dong H, et al. Construction of homologous cancer cell membrane camouflage in a nano-drug delivery system for the treatment of lymphoma. *J Nanobiotechnol* 2021;**19**:8.
2. Gong H, Zhang QZ, Komarla A, Wang SY, Duan Y, Zhou ZD, et al. Nanomaterial biointerfacing *via* mitochondrial membrane coating for targeted detoxification and molecular detection. *Nano Lett* 2021;**21**:2603−9.
3. Li S, Jiang WP, Yuan YP, Sui MJ, Yang YQ, Huang LQ, et al. Delicately designed cancer cell membrane-camouflaged nanoparticles for targeted F-19 MR/PA/FL imaging-guided photothermal therapy. *Acs Appl Mater Inter* 2020;**12**:57290−301.
4. Hu CMJ, Zhang L, Aryal S, Cheung C, Fang RH, Zhang LF. Erythrocyte membrane-camouflaged polymeric nanoparticles as a biomimetic delivery platform. *Proc Natl Acad Sci U S A* 2011;**108**:10980−5.
5. Patel RB, Ye MZ, Carlson PM, Jaquish A, Zangl L, Ma B, et al. Development of an *in situ* cancer vaccine *via* combinational radiation and bacterial-membrane-coated Nanoparticles. *Adv Mater* 2019;**31**:e1902626.
6. Bahmani B, Gong H, Luk BT, Haushalter KJ, DeTeresa E, Previti M, et al. Intratumoral immunotherapy using platelet-cloaked nanoparticles enhances antitumor immunity in solid tumors. *Nat Commun* 2021;**12**:1999.
7. Zhang G, Campbell GR, Zhang QZ, Maule E, Hanna J, Gao WW, et al. $CD4^+$ T cell-mimicking nanoparticles broadly neutralize HIV-1 and suppress viral replication through autophagy. *Mbio* 2020;**11**:e00903-e00920.
8. Mei D, Gong LD, Zou YR, Yang D, Liu HB, Liang YG, et al. Platelet membrane-cloaked paclitaxel-nanocrystals augment postoperative chemotherapeutical efficacy. *J Control Release* 2020;**324**:341−53.
9. Feng SN, Li H, Ren YJ, Zhi CY, Huang YX, Chen FX, et al. RBC membrane camouflaged boron nitride nanospheres for enhanced biocompatible performance. *Colloids Surf, B* 2020;**190**:110964.
10. Drews J. Drug discovery: a historical perspective. *Science* 2000;**287**:1960−4.
11. Rask-Andersen M, Almén MS, Schiöth HB. Trends in the exploitation of novel drug targets. *Nat Rev Drug Discov* 2011;**10**:579−90.
12. Imming P, Sinning C, Meyer A. Drugs, their targets and the nature and number of drug targets. *Nat Rev Drug Discov* 2006;**5**:821−34.
13. Hu Q, Jia LL, Zhang XL, Zhu AH, Wang SC, Xie XY. Accurate construction of cell membrane biomimetic graphene nanodecoys *via* purposeful surface engineering to improve screening efficiency of active components of traditional Chinese medicine. *Acta Pharm Sin B* 2022;**12**:394−405.

14. Hu Q, Bu YS, Cao RQ, Zhang G, Xie XY, Wang SC. Stability designs of cell membrane cloaked magnetic carbon nanotubes for improved life span in screening drug leads. *Anal Chem* 2019;**91**:13062−70.
15. Sherwood J, Sowell J, Beyer N, Irvin J, Stephen C, Antone AJ, et al. Cell-membrane coated iron oxide nanoparticles for isolation and specific identification of drug leads from complex matrices. *Nanoscale* 2019;**11**:6352−9.
16. Luk BT, Hu CMJ, Fang RH, Dehaini D, Carpenter C, Gao WW, et al. Interfacial interactions between natural RBC membranes and synthetic polymeric nanoparticles. *Nanoscale* 2014;**6**:2730−7.
17. Fan ZY, Zhou H, Li PY, Speer JE, Cheng H. Structural elucidation of cell membrane-derived nanoparticles using molecular probes. *J Mater Chem B* 2014;**2**:8231−8.
18. Hubbard SR, Till JH. Protein tyrosine kinase structure and function. *Annu Rev Biochem* 2000;**69**:373−98.
19. Paul MD, Grubb HN, Hristova K. Quantifying the strength of hetero-interactions among receptor tyrosine kinases from different subfamilies: implications for cell signaling. *J Biol Chem* 2020;**295**:9917−33.
20. Zhang X, Simons M. Receptor tyrosine kinases endocytosis in endothelium biology and signaling. *Arterioscler Thromb Vasc Biol* 2014; **34**:1831−7.
21. Shao J, Markowitz JS, Bei D, An GH. Enzyme- and transporter-mediated drug interactions with small molecule tyrosine kinase inhibitors. *J Pharm Sci* 2014;**103**:3810−33.
22. Bu YS, Zhang XL, Zhu AH, Li LH, Xie XY, Wang SC. Inside-out-oriented cell membrane biomimetic magnetic nanoparticles for high-performance drug lead discovery. *Anal Chem* 2021;**93**:7898−907.
23. Ai XZ, Wang SY, Duan YO, Zhang QZ, Chen MS, Gao WW, et al. Emerging approaches to functionalizing cell membrane-coated nanoparticles. *Biochemistry* 2021;**60**:941−55.
24. Inui O, Teramura Y, Iwata H. Retention dynamics of amphiphilic polymers PEG-lipids and PVA-alkyl on the cell surface. *Acs Appl Mater Inter* 2010;**2**:1514−20.
25. Itagaki T, Arima Y, Kuwabara R, Kitamura N, Iwata H. Interaction between cells and poly(ethylene glycol)-lipid conjugates. *Colloids Surf B Biointerfaces* 2015;**135**:765−73.
26. Huang LL, Nie WD, Zhang JF, Xie HY. Cell-membrane-based biomimetic systems with bioorthogonal functionalities. *Acc Chem Res* 2020;**53**:276−87.
27. Wang DY, Zhang Y, Kleiner RE. Cell- and polymerase-selective metabolic labeling of cellular RNA with 2 ’-azidocytidine. *J Am Chem Soc* 2020;**142**:14417−21.
28. Xie R, Hong SL, Chen X. Cell-selective metabolic labeling of biomolecules with bioorthogonal functionalities. *Curr Opin Chem Biol* 2013;**17**:747−52.
29. Yoon HY, Koo H, Kim K, Kwon IC. Molecular imaging based on metabolic glycoengineering and bioorthogonal click chemistry. *Biomaterials* 2017;**132**:28−36.
30. Hu F, Yuan YY, Wu WB, Mao D, Liu B. Dual-responsive metabolic precursor and light-up AIEgen for cancer cell bio-orthogonal labeling and precise ablation. *Anal Chem* 2018;**90**:6718−24.
31. Han YT, Pan H, Li WJ, Chen Z, Ma AQ, Yin T, et al. T cell membrane mimicking nanoparticles with bioorthogonal targeting and immune recognition for enhanced photothermal therapy. *Adv Sci* 2019;**6**: 1900251.
32. Li WJ, Pan H, He HM, Meng XQ, Ren Q, Gong P, et al. Bio-orthogonal T cell targeting strategy for robustly enhancing cytotoxicity against tumor cells. *Small* 2019;**15**:e1804383.
33. Debets MF, Tastan OY, Wisnovsky SP, Malaker SA, Angelis N, Moeckl LKR, et al. Metabolic precision labeling enables selective probing of O-linked N-acetylgalactosamine glycosylation. *Proc Natl Acad Sci U S A* 2020;**117**:25293−301.
34. Chinoy ZS, Bodineau C, Favre C, Moremen KW, Durán RV, Friscourt F. Selective engineering of linkage-specific $\alpha$2,6-N-linked sialoproteins using sydnone-modified sialic acid bioorthogonal reporters. *Angew Chem Int Ed Engl* 2019;**58**:4281−5.
35. Braun AC, Gutmann M, Lühmann T, Meinel L. Bioorthogonal strategies for site-directed decoration of biomaterials with therapeutic proteins. *J Control Release* 2018;**273**:68−85.
36. Bu YS, Hu Q, Zhang XL, Li T, Xie XY, Wang SC. A novel cell membrane-cloaked magnetic nanogripper with enhanced stability for drug discovery. *Biomater Sci* 2020;**8**:673−81.
37. Fan XM, Shen JJ, Xu YY, Gao J, Zhang YW. Metabolic integration of azide functionalized glycan on Escherichia coli cell surface for specific covalent immobilization onto magnetic nanoparticles with click chemistry. *Bioresour Technol* 2021;**324**:124689.
38. Chen XF, Wu YL, Chen C, Gu YQ, Zhu CY, Wang SP, et al. Identifying potential anti-COVID-19 pharmacological components of traditional Chinese medicine Lianhuaqingwen capsule based on human exposure and ACE2 biochromatography screening. *Acta Pharm Sin B* 2021;**11**:222−36.
39. Gu YQ, Chen X, Wang Y, Liu Y, Zheng LY, Li XQ, et al. Development of 3-mercaptopropyltrimethoxysilane (MPTS)-modified bone marrow mononuclear cell membrane chromatography for screening anti-osteoporosis components from Scutellariae Radix. *Acta Pharm Sin B* 2020;**10**:1856−65.
40. Brown EJ, Frazier WA. Integrin-associated protein (CD47) and its ligands. *Trends Cell Biol* 2001;**11**:130−5.
41. Raju TS, Lang SE. Diversity in structure and functions of antibody sialylation in the Fc. *Curr Opin Biotechnol* 2014;**30**:147−52.
42. Ou HX, Chen QH, Pan JM, Zhang YL, Huang Y, Qi XY. Selective removal of erythromycin by magnetic imprinted polymers synthesized from chitosan-stabilized Pickering emulsion. *J Hazard Mater* 2015;**289**:28−37.
43. Nie L, Guo XJ, Esmailzadeh L, Zhang JS, Asadi A, Collinge M, et al. Transmembrane protein ESDN promotes endothelial VEGF signaling and regulates angiogenesis. *J Clin Invest* 2013;**123**:5082−97.